

# Watt-Level Wireless Power Transfer Based on Stacked Flex Circuit Technology

Xuehong Yu, Florian Herrault, Chang-Hyeon Ji, Seong-Hyok Kim, Mark G. Allen  
Gianpaolo Lisi\*, Luu Nguyen\*, and David I. Anderson\*  
Georgia Institute of Technology, Atlanta, GA, USA  
\*National Semiconductor Corporation, Santa Clara, CA, USA  
Email: xyu31@mail.gatech.edu

## Abstract

This paper presents the design, simulation, fabrication, and experimental characterization of a multi-layer spiral inductor that acts as the receiver coil for watt-level wireless power transfer. The inductor was designed with multiple vertical laminations where 88- $\mu\text{m}$ -thick copper coils were separated by 25- $\mu\text{m}$ -thick Kapton films using a flexible PCB fabrication technique. This Cu-Kapton approach has the potential for lower-cost coil fabrication than relatively expensive Litz-wire winding techniques. Varying turn widths were implemented to account for proximity effects and maximize the coil current distribution uniformity inside the coil windings at a given frequency, as validated by two-dimensional electromagnetic simulations. The multi-layer design incorporating lamination of four layers together with width variation exhibited a Q-factor improvement of 150% in comparison to the single-layer inductor. It was measured to have an inductance of 17  $\mu\text{H}$  and a Q-factor of 50 at 300 kHz with an outer diameter of 5 cm. With a Litz-wire inductor as the transmitter coil for wireless power transfer, a load power of 7 Watts was transferred at 300 kHz over a distance of 5 cm and 5 Watts over 10 cm, two times the coil diameter, achieving an overall efficiency (defined as the ratio of the received load power to the total input power to the driving circuitry) of 46% and 23% respectively. In comparison, a manually-wound Litz-wire receiver coil with same characteristics under similar conditions demonstrated an overall efficiency of 58% and 39% at one and two-diameter distances, respectively.

## Introduction

Wireless power transfer has recently gained significant interest as a potential approach for contactless battery charging [1] [2] as well as data transmission due to not only the ubiquitousness of portable and handheld devices, but also the development of distributed wireless sensor networks and implantable microsystems [3]. Successful powering of cell phones [4] and desktop peripheral applications [5] has been demonstrated where the application device was equipped with receiver coils and wirelessly charged when being coupled closely to the transmitter coils. The mechanism behind this, referred to as “inductive coupling,” is that the current in the transmitter coils generates an alternating electromagnetic field, which then interacts with the receiver coils to generate a current or voltage-drop in it. Although attractive, this mechanism is most appropriate for transferring energy over a very small distance [1] [2] [5], compared to the size of the coils.

Unlike inductive coupling, resonant energy transfer [4], which is based on frequency matching and high-Q transmitter and receiver coil designs, theoretically enables efficient power transfer over large distances, e.g., for up to several coil

diameters. Due to its resonance nature, energy will be coupled mostly to objects of the same resonant frequency and less to off-resonant objects. Further, due to the high Q-factor design, there is reduced resistive loss in the circuits, which therefore leads to reasonably efficient mid-range wireless power transfer. In contrast to the close-range power transfer using inductive coupling, mid-range wireless power transfer is typically implemented over distances ranging from two to ten times the inductor size. Results in [6] showed that a transfer efficiency of approximately 40%-50% could be attained through resonant coupling between two helical coils for a distance up to 4 times the coil diameter at an operating frequency of 9.9 MHz. The helical coils had a size of 60 cm in diameter, a height of 20 cm, a wire radius of 3 mm, and measured 950 in Q-factor. The overall efficiency fell to 15% when the entire system was considered, in which 60 W out of 400 W input power was transferred to the load. Another resonant power transfer system using two spiral coils with moderate sizes was demonstrated in [7], where a transfer efficiency of 25% and 4% was achieved at 30 MHz between a 24-cm-diameter coil pair for a distance of 10 cm and 50 cm, respectively. Similar measurements for a 12-cm-diameter coil pair yielded a transfer efficiency of 16.5% and 2.5% respectively. The relatively low efficiency obtained was due to the low Q-factors of the transmitter and receiver coils plus the weak coupling between them.

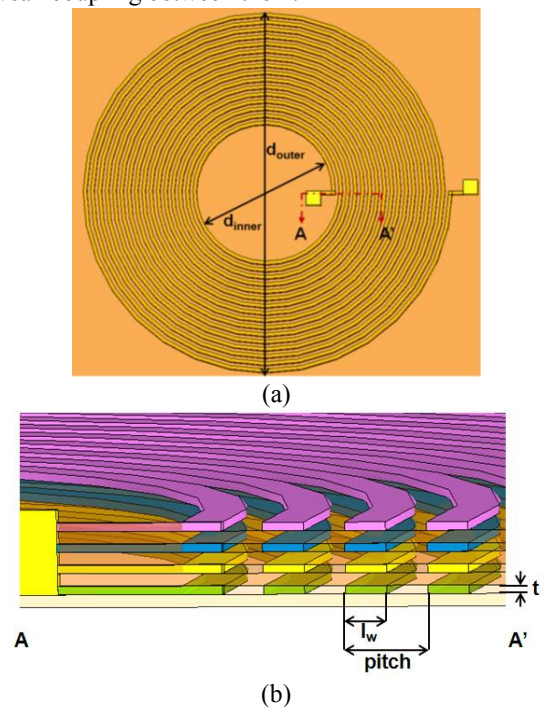


Figure 1: Schematic of the multi-layer spiral inductor, (a) top view, and (b) partial cross-sectional view.

In this paper, the goal is to develop a low-profile receiver coil that is suitable for applications requiring multi-watt power levels using mid-range wireless power transfer. The footprint of the coil is confined to a 5 cm by 5 cm region, considering its potential application in consumer electronics, and a spiral design (Figure 1) is chosen due to its straightforward integration. The receiver coil is designed with multiple vertical laminations and varying turn widths to maximize the Q-factor. Axisymmetric two-dimensional (2-D) electromagnetic simulations are performed to verify the design. The use of flexible printed-circuit-board (PCB) fabrication techniques potentially enables not only relatively low-cost manufacturing, but also conformable and space-efficient incorporation of coils into more complicated systems. Experiments measuring coil performance as well as demonstrating wireless power transfer are conducted, and performance characteristics of each are given. Although the operating frequency is fixed to 300 kHz in this work, the method presented is applicable to other frequencies.

### Wireless Power Transfer Circuit Analysis

A simplified schematic of a typical setup for wireless power transfer is shown in Figure 2, where  $V_s$  represents an ideal power source,  $R_L$  is the load resistance to which power will be wirelessly transferred,  $M$  is the mutual inductance between the coupled transmitter and receiver coil inductors  $L_1$  and  $L_2$ ,  $C_1$  and  $C_2$  are the series capacitances utilized to set the resonant frequency for power transfer (with  $\frac{1}{L_1 C_1} = \omega_0^2$  and  $\frac{1}{L_2 C_2} = \omega_0^2$ ), and  $R_1$ ,  $R_2$  are parasitic resistances.

The power transfer efficiency,  $\eta$ , at resonance is defined as the power absorbed by the load divided by the total input power extracted from the power source, which is formulated as [8]:

$$\eta = \frac{\omega_0^2 M^2 R_L}{(R_2 + R_L)^2 Z_1} \quad (1),$$

$$Z_1 = R_1 + \frac{\omega_0^2 M^2}{(R_2 + R_L)} \quad (2),$$

where  $\omega_0$  is the circuit resonant frequency, and  $Z_1$  is the impedance seen by the power source  $V_s$  that incorporates the effect of the load resistance when the receiver coil is coupled to the transmitter coil. To gain better insight into the circuit, equation (1) is combined with equation (2) and rearranged as:

$$\eta = \frac{R_L}{R_2 + R_L} \cdot \frac{\omega_0^2 M^2}{R_1 (R_2 + R_L) + \omega_0^2 M^2} \quad (3).$$

In the case of an ideal transmitter coil that has no resistive loss and is coupled only to the receiver coil,  $R_1 = 0$  and  $Q_1 = \infty$ , the transfer efficiency, denoted as  $\eta_\infty$ , reduces to:

$$\eta_\infty = \frac{R_L}{R_2 + R_L} \quad (4),$$

which depends only on the receiver circuits. If the receiver coil also has zero resistance and infinite  $Q_2$  as in an ideal case, the transfer efficiency becomes independent of the mutual inductance and the load (this unrealistic case is due to the assumptions of ideal drive source and zero parasitics; although no real power is lost, significant reactive power will be present in the circuits). In reality, resistive loss is present in the inductor, and it has a finite Q-factor value. In such a case, the transfer efficiency can be represented as an ideal efficiency for the case of an ideal transmitter coil,  $\eta_\infty$ , times

an attenuation factor determined by the Q-factors and the coupling effect:

$$\eta = \eta_\infty \cdot \frac{1}{1 + \frac{1}{k^2 Q_1 Q_{2,1}}} \quad (5),$$

where  $k$  is the coupling coefficient with  $M = k\sqrt{L_1 L_2}$ ,  $Q_1$  is the unloaded Q-factor of the transmitter coil with  $Q_1 = \frac{\omega_0 L_1}{R_1}$ , and  $Q_{2,1}$  is the loaded Q-factor of the receiver coil, defined as  $Q_{2,1} = \frac{\omega_0 L_2}{R_2 + R_L}$ . Clearly, for a given load, the key factors for enabling high power transfer efficiency are a high unloaded Q-factor of the transmitter coil, high loaded Q-factor of the receiver coil, and a high coupling coefficient between them.

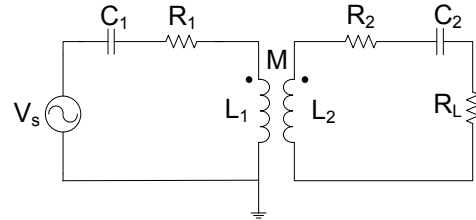


Figure 2: Simplified schematic of a typical setup for wireless power transfer.

### Inductor Design and Simulation Results

As discussed above, one of the key factors for enabling efficient resonant power transfer is the high Q-factor of the receiver coil, given that the transmitter and receiver coils have been tuned to operate at the same resonant frequency. The Q-factor of a spiral inductor can be calculated from its inductance and resistance at a given frequency:

$$Q = \frac{\omega L}{R_\omega} \quad (6),$$

where  $\omega$  is the angular frequency,  $L$  is the inductance, and  $R_\omega$  is the overall resistance of the inductor at the target frequency.

To design a receiver coil, the specific application will dictate choices of critical parameters such as inductance value and coil diameter. Other parameters can then be chosen to maximize the quality factor. For spiral inductors, the inductance at low frequency in the absence of permeable material can be approximated well using the formula in [9]:

$$L_s = \frac{\mu_0 n^2 d_{avg}}{2} \left( \ln \left( \frac{2.46}{\rho_s} \right) + 0.2 \rho_s^2 \right) \quad (7),$$

where  $\mu_0$  is the permeability of free space,  $n$  is the number of total turns in the inductor,  $d_{avg}$  is the average diameter of the inductor with  $d_{avg} = (d_{outer} + d_{inner})/2$ , where  $d_{outer}$  is the diameter of the outermost turn and  $d_{inner}$  is the diameter of the innermost turn, and  $\rho_s$  is a geometrical fill ratio defined by  $(d_{outer} - d_{inner})/(d_{outer} + d_{inner})$ . Since practical circuit considerations limit the voltage levels in the coils, these voltage limits translate into a limit on the coil inductance values in our system on the order of tens of microhenries. Further, the dimensions of the windings can be chosen to be on the order of twice the skin depth as a rule of thumb, resulting in the pitch between turns, as defined in Figure 1, to be on the order of hundreds of micrometers. The outer diameter of the inductor is fixed due to the footprint requirement of the application. Once these parameters have been chosen, equation (7) can be used to determine the total number of turns.

The resistance of the inductor includes two parts: dc resistance and ac resistance:

$$R_w = R_{dc} + R_{ac} = R_{dc}(1 + \alpha_{ac}) \quad (8).$$

By approximating all spiral windings to be concentric circles, the equations describing dc resistance are formulated as:

$$R_{dc} = \frac{\rho l}{l_w t} \quad (9),$$

$$l = \frac{\pi n(d_{outer} + d_{inner})}{2} \quad (10),$$

$$d_{inner} = d_{outer} - 2n(l_w + l_g) \quad (11),$$

where  $\rho$  is the resistivity of copper,  $l$  is the total length of all the turns in the inductor,  $l_w$  is the width of a single turn,  $l_g$  is the gap between turns, and  $t$  is the thickness of the turns.

The ac resistance models the skin depth effect and proximity effect inside the wires at high frequencies, and a function  $\alpha_{ac}$  is used to denote the dependency of ac resistance on parameters such as frequency, skin depth, copper thickness, turn number, turn width and turn pitch [10] [11] [12].

By substituting equations (8)-(11) into equation (1), the Q-factor becomes:

$$Q = \frac{1}{1 + \alpha_{ac}} \cdot \frac{\omega L}{\pi \rho} \cdot l_w \cdot t \cdot \frac{1}{n(d_{outer} - n(l_w + l_g))} \quad (12).$$

First, the effect of the dc resistance on the Q-factor will be discussed analytically, followed by simulations to determine the effect of ac resistance (i.e., the magnitude of the expression  $\frac{1}{1 + \alpha_{ac}}$ ). Since the inductance value and the outer diameter of the coil are fixed, the pitch between turns determines the total number of turns, as discussed before. Thus, for a given pitch, the turn number is also a constant, and what remains in equation (12) are only the turn width and the winding thickness. Because of the linear relationship between Q-factor and the turn width, an optimized Q-factor can be obtained with a maximized turn width, which is, however, practically limited by how small the gap could be realized through fabrication processes. Similar constraints exist for the winding thickness. Although the thicker the copper, the higher the Q-factor, fabrication and technology constraints determine the maximum thickness that can be achieved.

Thus, for a given number of turns prescribed by the required inductance, together with other factors mentioned above, the Q-factor can be optimized by determining the optimal pitch and turn width. However, with a single-layer design, the improvement available from varying these parameters is limited. To address this issue, a vertical lamination concept is proposed to overcome the overall area constraints to further increase the Q-factor, as shown in Figure 1. In addition, we utilized the concept of a varying width design to further reduce losses, as shown in Figure 3. To achieve the vertical lamination, optimized single-layer inductors with varying turn widths are stacked together and separated by thin layers of Kapton film. The multiple inductor layers are then connected in parallel to reduce the resistance of the overall inductor. Due to the almost perfect coupling between adjacent layers, the overall inductance of the laminated inductor remains the same as a single-layer inductor since the added mutual inductance between layers compensates for the reduction in inductance resulting from a parallel-connected configuration.

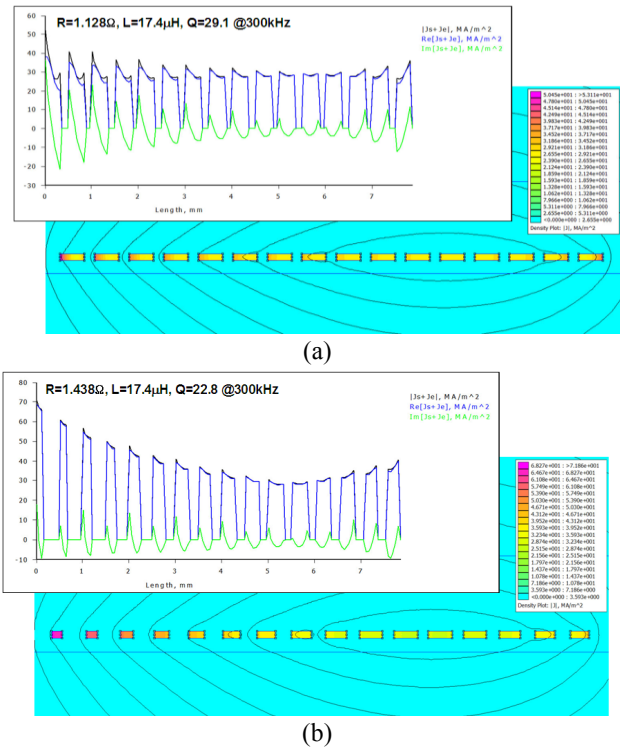


Figure 3: Current density distribution for a single-layer 16-turn inductor with (a) uniform turn width of 350  $\mu\text{m}$  and (b) variable turn width ranging from 150  $\mu\text{m}$  to 350  $\mu\text{m}$ . Both have a constant turn pitch of 500  $\mu\text{m}$ .

2-D electromagnetic simulations using the simulation package FEMM were conducted to determine the optimized current density distribution inside the turns for varying width designs. Figure 3 shows a comparison between the original design with uniform turn width and a design with varying turn width. The inductor with uniform width design does not have uniform current distribution throughout the cross-section of each turn. For example, the 5th turn from inner end have the most uniform current distribution while the turns farthest from it suffer from severe proximity effect, which creates the large current peaks near the boundaries of the windings. To suppress this eddy current loss, the width of each turn is modified as shown in the figure. Starting from the position of minimum proximity effect and going to the inner and outer edge of the coil, the width of each turn is reduced gradually by 20  $\mu\text{m}$  while the pitch between turns is fixed. A better uniformity in the current density distribution is achieved with no obvious current peaks near the boundaries. The high current density value is due to the reduced cross-section of the windings. Although the Q-factor of a single layer inductor with variable width is typically lower than that of a constant width design, as will be seen later, this effect is reversed for stacked layers.

An optimized design was then found through finite element simulations for different combinations of turn width and gap values using varying width design, as shown in Table I. The simulated inductor has a four-layer lamination with a vertical inter-layer gap of 125  $\mu\text{m}$ , and each layer has an outer diameter of 5 cm, a copper thickness of 100  $\mu\text{m}$ , and a turn number of 16. The turn width varies from 250  $\mu\text{m}$  to

350  $\mu\text{m}$ , as shown in the table, and the gap between turns varies from 50  $\mu\text{m}$  to 150  $\mu\text{m}$ . For a constant pitch, as the diagonal line indicates in the table, the Q-factor increases with an increasing width and shrinking gap, which agrees well with the analytical result. The maximum Q is obtained with a combination of 350  $\mu\text{m}$  width and 50  $\mu\text{m}$  gap, which is, however, not realistic because of the fabrication constraints. Therefore, an optimized design with the turn width of 350  $\mu\text{m}$  and gap of 150  $\mu\text{m}$  was selected and implemented in this paper. It should be noted that the fabricated coils were 88  $\mu\text{m}$  thick, causing the Q-factor to be smaller than the simulated values presented in Table I.

To study the effectiveness of multilayer lamination in improving Q-factor, simulations for parallel-connected inductors with various numbers of lamination layers were also performed. The results are given in Figure 4. The Q-factor of the inductor increased from approximately 20 for a single-layer inductor with varying width design to more than 55 with the added second and third laminations, showing almost 200% improvement. However, a saturating trend was observed after stacking more than 4 layers, and the improvement in Q-factor upon increasing layers becomes negligible. This is largely due to the increased ac resistance of the inductor, which likely results from the increased proximity effects of the added layers, despite the fact that the dc resistance continues to decrease with additional laminations.

Table I: Simulated Q-factor, resistance and inductance values for varying width inductors with different geometrical design. The diagonal line in the first table represents designs with constant pitch. The Gap and width values are the original values before applying variable width design.

Gap/Width [ $\mu\text{m}$ ]		Gap [ $\mu\text{m}$ ]		
		50	100	150
Width [ $\mu\text{m}$ ]	250			$R_{dc}=0.461\Omega$ $R_{250}=0.530\Omega$ $L=19.1\mu\text{H}$
	300	$R_{dc}=0.415\Omega$ $R_{300}=0.524\Omega$ $L=20.1\mu\text{H}$	$R_{dc}=0.406\Omega$ $R_{300}=0.493\Omega$ $L=18.8\mu\text{H}$	$R_{dc}=0.401\Omega$ $R_{300}=0.590\Omega$ $L=17.7\mu\text{H}$
	350	$R_{dc}=0.367\Omega$ $R_{350}=0.477\Omega$ $L=18.7\mu\text{H}$		$R_{dc}=0.353\Omega$ $R_{350}=0.428\Omega$ $L=16.6\mu\text{H}$

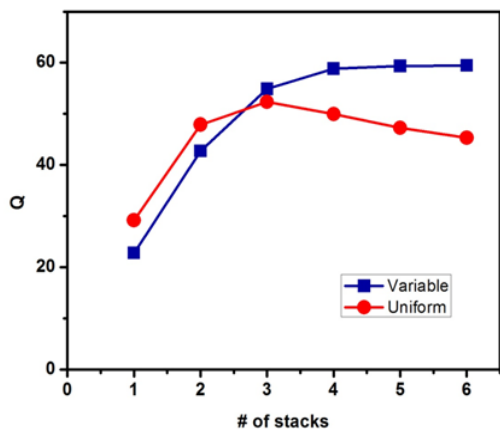


Figure 4: Simulation results of Q-factor vs. number of parallel-connected stacked layers for uniform and variable width design at 300 kHz.

## Inductor Fabrication and Characterization Results

To fabricate the inductor design consisting of laminated coil layers, a low-cost fabrication process based on a flexible PCB technique was proposed, as shown in Figure 5. A commercially available flexible Kapton film with copper layer on top was first coated with a photo-definable resist and patterned using a standard photolithography process in step (a). Wet etching was then performed in step (b) to etch away the copper exposed from the photoresist pattern and define the coil windings. Due to the isotropic characteristics of the wet etching process, the cross-section of the generated coils was more of a trapezoidal shape with curved sidewalls rather than a rectangular shape. After removal of the photoresist, electroplating was conducted in step (c) to further increase the copper thickness of the windings. Since electroplating is also an isotropic process, copper grew on top of the windings as well as on the sidewall and compensated for the possible size loss coming from previous wet etching process. After multiple single-layer coils had been fabricated, a vertically laminated inductor was completed by alignment and stacking, followed by definition of electrical interconnects between layers. Pictures of the fabricated single and multi-layer inductors are shown in Figure 6. The use of flexible PCB substrates enables not only a fast and easy process with low cost, but also an inductor with flexible and low profile, which favors space-efficient incorporation of the coils into complex systems.

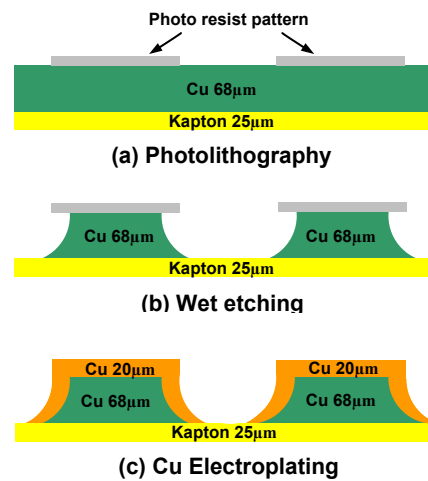


Figure 5: Fabrication process using flexible PCB technique

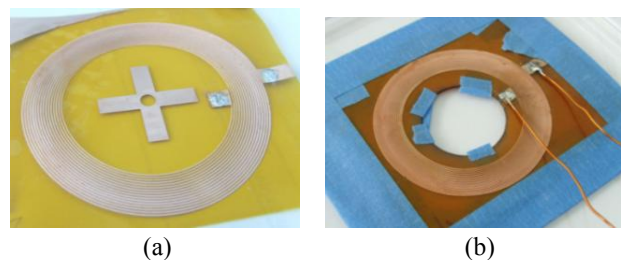


Figure 6: Fabricated spiral inductors with (a) single layer and (b) four stacked layers.

An impedance analyzer (HP4194) was used to characterize the resistance, inductance, and Q-factor for both single and multi-layer inductors. Results for single-layer inductors are given in Figure 7, where Coil1 to Coil4 represent four different inductors that will be laminated together. The resistance, as plotted in dashed lines, increases with frequency due to the increased eddy current loss and proximity effect at high frequencies. The measured inductance values of different coils are reasonably close and remain stable at approximately  $17\ \mu\text{H}$  for frequencies up to 1 MHz. The small discrepancies in values resulted from imperfectly patterned windings due to the fabrication tolerances. The Q-factors reach 20 at 300 kHz and increase linearly with frequency. Characterization results for the four-layer inductor assembled using the four single-layer inductors are shown in Figure 8, where the resistance is reduced to  $0.6\ \Omega$  at 300 kHz while the inductance value only experiences a small decrease from  $17\ \mu\text{H}$  to  $16.3\ \mu\text{H}$ . As a result, the Q-factor reaches 50.1 at 300 kHz, which is more than two times that of the original single-layer inductors. To validate the relationship between the lamination approach and the inductor performance, the Q-factors for inductors with various laminated layers were also measured and compared with the simulation results given before, as shown in Figure 9. The three plots in the figure represent the Q-factors obtained from experimental results, previous simulation results using an ideal sidewall geometry model, and new simulation results using a trapezoidal sidewall model. As stated in the fabrication section, the cross-section of the coil winding is closer to a trapezoid rather than an ideal rectangular shape. Trapezoidal-shaped sidewalls match the experimental trend with an overall error of less than 10%. The discrepancy error mainly comes from the imperfectly fabricated devices, such as variation in winding width and gap definition, misalignment of vertical laminations, etc.

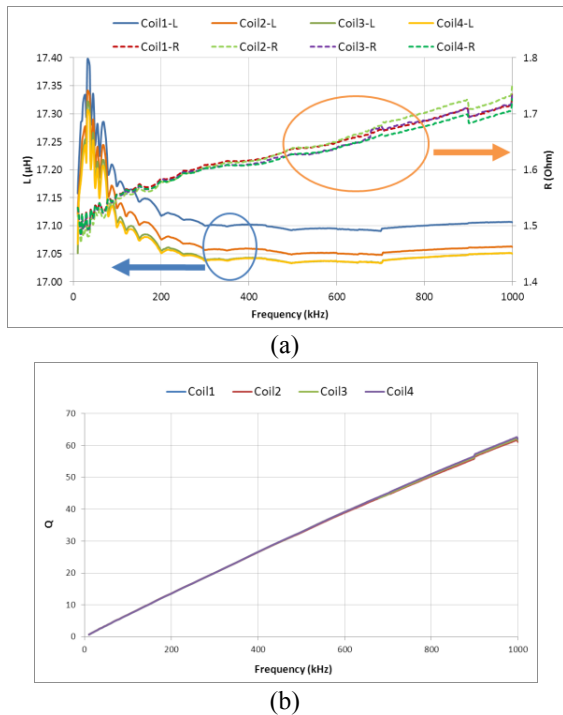


Figure 7: Characterization results for single-layer inductors, (a) resistance and inductance, (b) Q-factor.

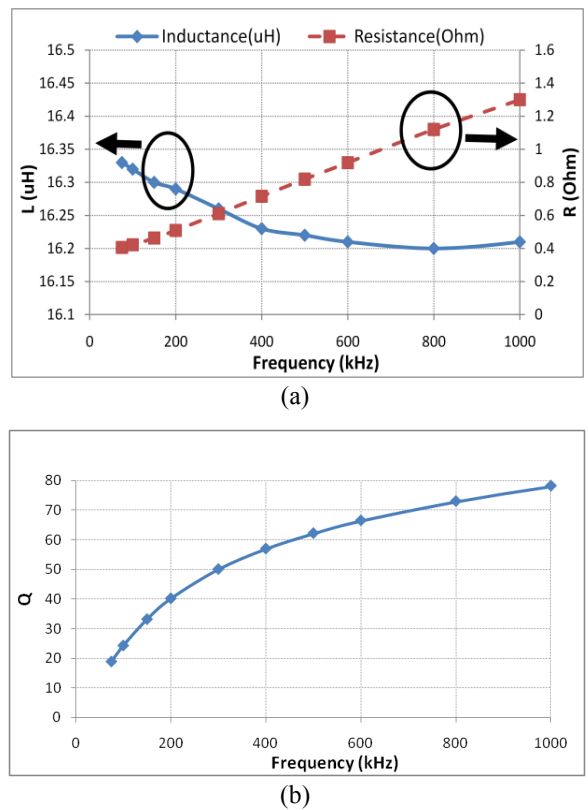


Figure 8: Characterization results for the four-layer inductor, (a) resistance and inductance, (b) Q-factor.

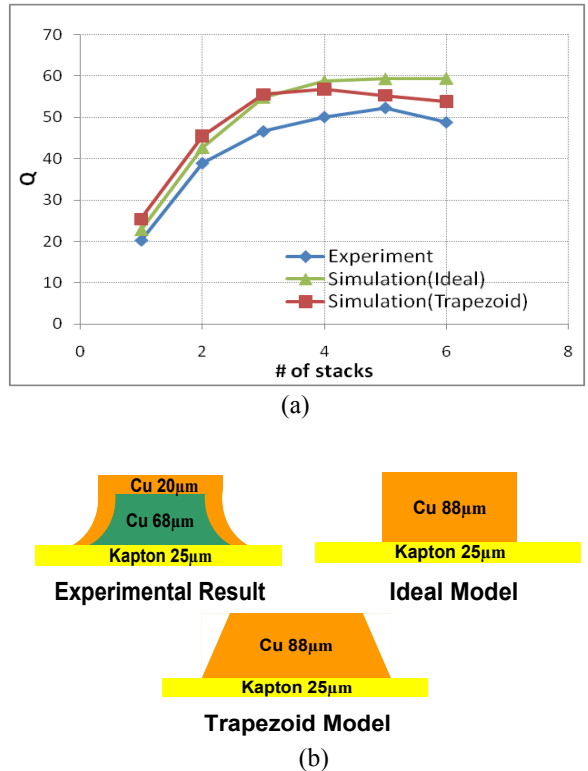


Figure 9: Measured Q-factor for various laminated layers in (a) with the simulation models shown in (b).

### Wireless Power Transfer Testing Results

With the high Q-factor design for the receiver coil completed, the key factors remaining for enabling efficient wireless power transfer are the Q-factor of the transmitter coil and the coupling coefficient between the transmitter and receiver coil. Since the size of the transmitter coil is not as critical as the receiver coil in our application, a relatively large transmitter coil with a high Q-factor can be used. The experimental setup for resonant wireless power transfer is shown in Figure 10, where on the transmitter side, an AC-DC converter is connected through an H-bridge to supply the desired ac signal from the grid, and a frequency-tuning component with control circuits is used to tune the resonant frequency of the transmitter coil. The transmitter coil is a Litz-wire coil with an outer diameter of 20 cm, an inductance value of 45.4  $\mu$ H, and a high Q-factor of 847 at 300 kHz. It was automatically tuned to operate at the resonant frequency of 300 kHz with a peak voltage limit of 500 V. The multi-layer spiral inductor acts as the receiver coil with frequency tuning circuits, and voltage regulator as well as rectifier is used to deliver the power to the ultimate load. The receiver coil was manually tuned to approach the transmitter's resonant frequency to maximize the power transfer efficiency.

A simplified schematic model for the system is shown in Figure 11, where  $V_s$  represents the input power source,  $R_s$  represents the resistance of the power source,  $C_{s1}$ ,  $C_{s2}$ ,  $C_{p1}$ , and  $C_{p2}$  are the tuning capacitances added in series or in parallel with the inductors for achieving resonance,  $C_s = \frac{1}{L_s \cdot \omega_0^2}$  and  $C_p = \frac{1}{L_p \cdot \omega_0^2}$ ,  $R_{Cs1}$ ,  $R_{Cs2}$ ,  $R_{Cp1}$ , and  $R_{Cp2}$  are the resistances of the corresponding capacitors,  $L_{s1}$  and  $L_{s2}$  are the leakage inductances of a transformer model representing the transmitter and receiver coil,  $L_p$  is the mutual inductance,  $R_1$ ,  $R_2$  are the resistances of the coils, and  $R_L$  is the load resistance.

The power transfer efficiency,  $\eta_t$ , which describes the direct energy transfer between the transmitter and receiver coils, as discussed in equation (1), is measured as the ratio of the power received in the receiver coil to the power sent out from the transmitter coil:

$$\eta_t = \frac{V_{out} I_{out}}{V_{in} I_{in}} \quad (13),$$

where  $V_{in}$  and  $V_{out}$  are the voltage labeled in Figure 11, and  $I_{in}$  and  $I_{out}$  are the current flowing in the segment corresponding to  $V_{in}$  and  $V_{out}$ .

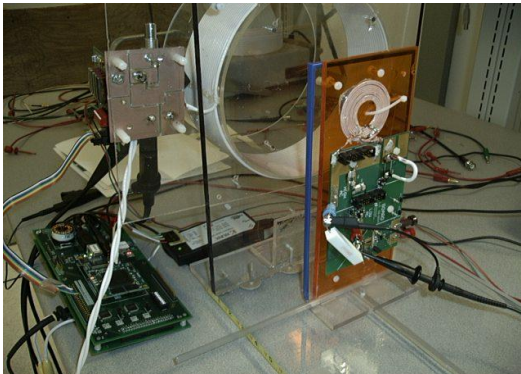


Figure 10: Picture of test setup for resonant power transfer.

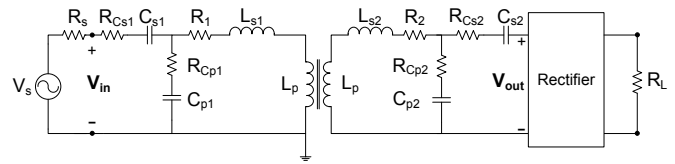


Figure 11: Schematic diagram of the test circuits for wireless power transfer.

When considering the entire system, an overall efficiency can be obtained, which describes the percentage of the power received on the load compared to the total input power from the power source.

The separation between the coils was adjustable along their axis, thus measurements were performed across an adjustable load for several different distances, with the results plotted in Figure 12. The transfer efficiency, as well as the overall efficiency, is shown as solid line with the reference axis on the left, and the actual power received on the load is shown as the dashed line with the reference axis on the right. Over a one-coil-diameter distance of 5 cm, a load power of 7 Watts is transferred at an overall efficiency of 46%, and at a two-coil-diameter distance of 10 cm, a load power of more than 5 Watts is successfully transferred, with an overall efficiency of 23% and a transfer efficiency of 33%. As the distance increases, the efficiency reduces, and at the distance larger than 20 cm, the efficiency drops to less than 5%. In comparison, a Litz-wire receiver coil with the same characteristics was also tested under similar conditions, and the results are shown in Figure 13, where an overall efficiency of 58% and 39% are demonstrated at one and two-diameter distances respectively.

The coupling efficient between the transmitter and multi-layer receiver coil was also calculated from the measurement data using:

$$k = \frac{L_m}{\sqrt{L_1 L_2}} = \frac{V_{2,pk}}{\omega_0 L_{1,pk} \sqrt{L_1 L_2}} \quad (14),$$

where  $\omega_0$  is the resonant frequency,  $L_m$  is the mutual inductance,  $V_{2,pk}$  is the peak voltage measured in the receiver coil, and  $I_{1,pk}$  is the peak current measured in the transmitter coil. A coupling coefficient of 0.42 was obtained at the distance of 10 cm, and 0.2 at the distance of 15 cm, as shown in Figure 14.

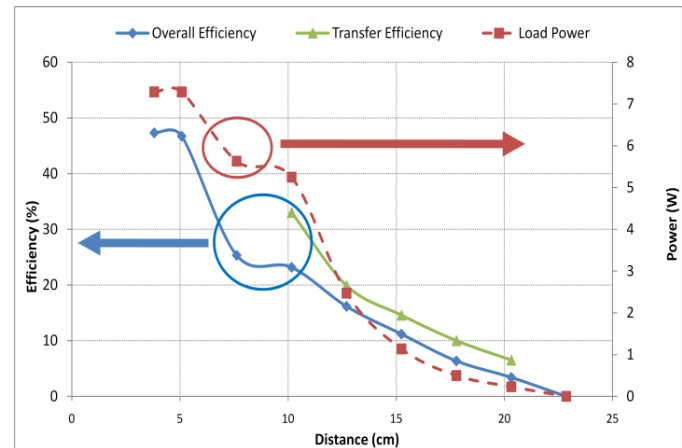


Figure 12: Measured load power, overall efficiency, and transfer efficiency for the multi-layer receiver coil.

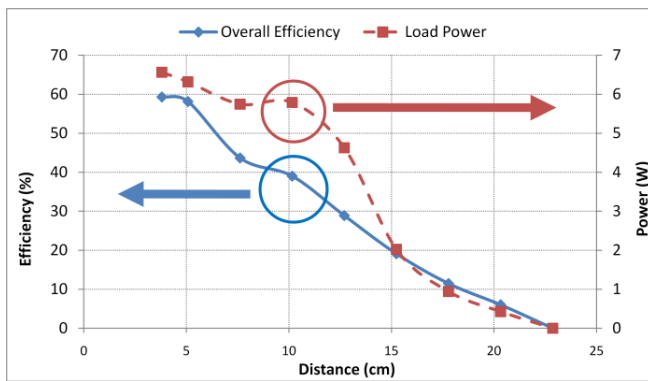


Figure 13: Measured load power and overall efficiency for the Litz-wire receiver coil.

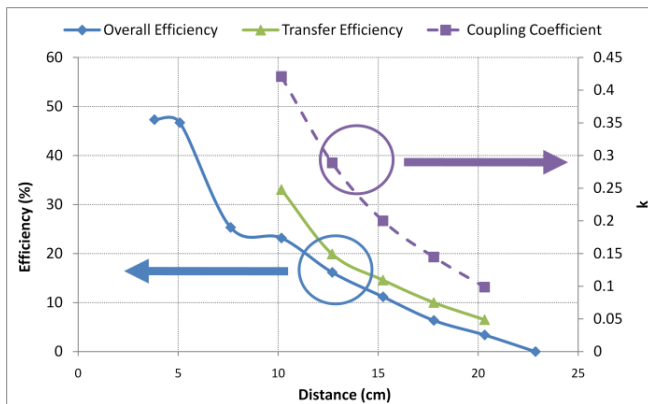


Figure 14: Measured overall efficiency, transfer efficiency and the coupling coefficient for the multi-layer receiver coil.

## Conclusions

A low-profile inductor with varying width design and vertical laminations was presented and watt-level efficient wireless power transfer over large distances was demonstrated through resonant inductive coupling. The special design of the inductor with high Q-factor and the strong coupling between the transmitter and receiver coils contributed to the improved efficiency in wireless power transfer despite the reduced profile of the receiver coil. The electromagnetic simulation performed provided insights into the inductor design with a prediction error of less than 10%.

## References

- Hui, S. Y. R., Ho, W. C., "A New Generation of Universal Contactless Battery Charging Platform for Portable Consumer Electronic Equipment," *35th Annual IEEE Power Electronics Specialists Conference*, Aachen, Germany, 2004, pp. 638 – 644.
- Sonntag, C. L. W., Lomonova, E. A., Duarte, J. L., and Vandenput, A. J. A., "Specialized Receivers for Three-Phase Contactless Energy Transfer Desktop Applications," *European Conference on Power Electronics and Applications*, Sept. 2007, pp.1-11.
- Wang, G., Liu, W., Sivaprakasam, M., Kendir, G. A., "Design and Analysis of an Adaptive Transcutaneous Power Telemetry for Biomedical Implants," *IEEE*

- Trans-Circuits and Systems-I*, Vol. 52, No. 10 (2005), pp. 2109-2117.
- Selvakumaran, R., Liu, W., Soong, B.H., Luo, Ming, Loon, S.Y., "Design of inductive coil for wireless power transfer," *IEEE/ASME International Conference on Advanced Intelligent Mechatronics*, July 2009, pp.584-589.
- Meyer, P., Germano, P., Markovic, M., Perriard, Y., "Design of a Contactless Energy Transfer System for Desktop Peripherals," *Energy Conversion Congress and Exposition (ECCE)*, Atlanta, GA, Sept. 2010, pp. 2253 – 2258.
- Kurs, A., Karalis, A., Moffatt, R., Joannopoulos, J. D., Fisher, P., Soljacic, M., "Wireless Energy Transfer via Strongly Coupled Magnetic Resonances," *Science*, Vol. 317, No. 5834 (2007), pp. 83-86.
- Mazlouman, S.J., Mahanfar, A., Kaminska, B., "Mid-range Wireless Energy Transfer using Inductive Resonance for Wireless Sensors," *ICCD*, Lake Tahoe, CA, Oct. 2009, pp.517-522.
- De Boeij, J., Lomonova, E., Vandenput, A., "Contactless Energy Transfer to a Moving Load Part I: Topology Synthesis and FEM simulation," *IEEE International Symposium on Industrial Electronics*, July 2006, vol.2, pp.739-744.
- Mohan, S.S., del Mar Hershenson, M., Boyd, S.P., Lee, T.H., "Simple Accurate Expressions for Planar Spiral Inductances," *IEEE Journal of Solid-State Circuits*, Vol. 34, No. 10 (1999), pp.1419-1424.
- Yue, C.P., Wong, S.S., "Physical modeling of spiral inductors on silicon," *IEEE Transactions on Electron Devices*, vol.47, no.3(2000), pp.560-568.
- Hu, Y. Q., Cheng, D. K. W., Lee, Y.S., "New fabrication method for planar multilayer windings used in low-profile magnetic components," *IEEE Transactions on Magnetics*, vol.35, no.2(1999), pp.1055-1059.
- Kuhn, W., Ibrahim, N., "Analysis of current crowding effects in multiturn spiral inductors," *IEEE Trans. Microw. Theory Tech*, vol. 49, no. 1(2001), pp. 31-38.